

## LUCIA, a microfocus soft XAS beamline

A.-M. Flank<sup>a,\*</sup>, G. Cauchon<sup>a</sup>, P. Lagarde<sup>a</sup>, S. Bac<sup>b</sup>, M. Janousch<sup>b</sup>, R. Wetter<sup>b</sup>,  
J.-M. Dubuisson<sup>c</sup>, M. Idir<sup>c</sup>, F. Langlois<sup>c</sup>, T. Moreno<sup>c</sup>, D. Vantelon<sup>c</sup>

<sup>a</sup> LURE, Bât. 209D, Centre Universitaire, BP 34, F-91898 Orsay, France

<sup>b</sup> Paul Scherrer Institut, SLS, Villigen-PSI, CH 5232, Switzerland

<sup>c</sup> SOLEIL, BP 48, F-91192 GIFYvette, France

Available online 25 January 2006

### Abstract

The beamline “LUCIA” (line for ultimate characterization by imaging and absorption) is a “tender” (0.8–8 keV) X-ray microprobe with capabilities for chemical speciation by micro-X-ray absorption spectroscopy ( $\mu$ -XAS) and for elemental mapping by X-ray micro-fluorescence ( $\mu$ -XRF). It allows the possibility to study heterogeneous samples at a micrometer scale and to combine these two element-specific and non-destructive techniques. A monochromatic beam of a few micrometer in size is incident on a sample which is mounted on a scanning  $x$ - $y$ - $z$  stage.  $\mu$ -XRF shows the location of the elements, their relative abundances, and their association with other elements. One can take advantage of the monochromatic beam which allows separating out different elements by their absorption edges. After mapping the fluorescence, spots of interest can be analysed by XAS to determine the speciation (local chemistry, quantitative determination of the local geometric structure around the absorbing atom) of the elements and how they depend on the different components.

Installed at first at the SLS of the Paul Scherrer Institute (Switzerland), the LUCIA beamline will be transferred to SOLEIL by the beginning of 2008. The energy range offered by the beamline corresponds to the best performances of SLS and SOLEIL in terms of brightness. It allows XAS experiments at the K edge of elements ranging from Na to Fe, L edges from Ni to Gd, and M edges of rare earths and actinides.

© 2005 Elsevier B.V. All rights reserved.

PACS: 07.85.Qe; 78.55.Qr; 78.70.Dm; 78.70.En; 79.60.Ht

Keywords:  $\mu$ -XRF;  $\mu$ -XAS; Element speciation; XAS under high pressure; Soft X-ray beamline; Al K edge

### 1. Introduction

The so-called “tender” X-ray domain (from about 0.8 to 8 keV) gives access to most of the elements in the periodic table, as it deals with the K edges of low  $Z$  elements (from sodium up to iron), the L edges from nickel to gadolinium, and the M edges of lanthanides and actinides. It can be covered by a two-crystal monochromator with a resolving power of about 4000. LUCIA (line for ultimate characterization by imaging and absorption), takes advantage of the high brightness synchrotron radiation delivered by the SLS

(swiss light source) and of the “undulator gap scan” to produce an energy tunable X-ray microbeam in that energy range. The goal is to perform spatially resolved elemental determination via X-ray fluorescence spectroscopy ( $\mu$ -XRF) and spatially resolved chemical speciation via X-ray absorption spectroscopy ( $\mu$ -XAS). It offers a large field in the quantitative and non-destructive elemental analysis of micro-heterogeneous materials. Its applications cover scientific domains from geosciences, to environmental and material sciences. Furthermore, taking advantage of the small size of the X-ray spot and of the high photon density, very demanding experiments in terms of sample environment, like high pressure X-ray absorption spectroscopy at low energy, become performable. This paper describes the beamline design and performance.

\* Corresponding author. Tel.: +41 56 3105307; fax: +41 56 3104551.  
E-mail address: [anne-marie.flank@psi.ch](mailto:anne-marie.flank@psi.ch) (A.-M. Flank).

## 2. Design of the beamline

Fig. 1 presents an overview of the LUCIA beamline located on the X07MA port at the SLS storage ring.

The source is an undulator of the APPLE-II type with a magnetic structure made of 32 magnets and a period of 54 mm [1]. Through a horizontal shift of the magnetic jaws, linearly polarized light from horizontal to vertical can be obtained as well as a circularly polarized beam. The size of the source is  $200 \times 20 \mu\text{m}^2$  (H  $\times$  V, FWHM).

The first optical element after the front end is a spherical mirror (incidence angle =  $0.4^\circ$ ) which provides a virtual focused horizontal source onto a set of adjustable slits. At this point, and according to calculations, the image of the source is  $86 \times 760 \mu\text{m}^2$  at a full aperture of the front-end slits. Following is a set of two flat mirrors with a variable incidence angle ( $0.4$ – $1.3^\circ$ ) which acts as a low-pass filter. This filter minimizes the contamination by high-order harmonics delivered by the undulator, and reduces the thermal load received on the monochromator crystals. All mirrors are pure silicon coated with 70 nm of nickel which has its L and K edges at respectively 860 and 8333 eV, therefore outside the energy domain of the beamline. They are water cooled. After each optical element, retractable beam monitors are installed. They allow to characterize the position and the intensity of the beam by means of a silicon diode, and of a YAG crystal. All the mirrors chambers of the beamline are under a vacuum in the  $10^{-9}$  mbar range, while the monochromator chamber vacuum, due to the mechanics inside, is only in the  $10^{-7}$  mbar region.

The choice of the double crystal monochromator (DCM) has been driven by the energy range of the beamline. This fixed exit beam monochromator is of the ‘‘Lemonnier cam type’’ [2]: the two crystals are mounted on a common shaft which provides the rotation, and the second

crystal translates to keep the exit beam at a constant height. Five pairs of crystals are available. They are positioned into the beam by a translation of the monochromator vessel which makes the change of the energy domain quite rapid. The first crystals are water-cooled. They are glued with an InGa eutectic layer to insure a good thermal contact. Special care is taken when illuminating these crystals to avoid thermal-shock degradation. The angular scanning range is from  $5^\circ$  to  $75^\circ$ , which puts the lower limit reachable with the Si(111) around 2040 eV. Below this energy, four sets of crystals are used, InSb(111),  $\text{YB}_{66}(400)$ ,  $\text{KTiOPO}_4(011)$  and beryls (10 $\bar{1}0$ ). The final focusing of the beam is achieved by a Kirkpatrick–Baez (KB) [3] system. It provides a high flux over a wide energy range, a stable beam position on the sample during an energy scan while giving a fairly large working distance. The performance of the focusing system is determined by the quality of the mirrors i.e. by the intrinsic rms slope errors and the rms surface roughness. With the aim to reduce the slope errors, two flat mirrors are elliptically bent. Based on a system developed at the ESRF [4], the benders have been designed to be UHV compatible, in order to avoid the absorption by the air in the low energy range. The mirrors are also made of Si and coated by nickel, and the incident angle is  $0.4^\circ$ . A motorized four-jaw entrance slit defines the horizontal and vertical acceptance of the KB. The working distance between the end of the last mirror and the focus is about 90 mm. In order to correct the small but nevertheless noticeable loss of parallelism of the two-crystals over the large angular working range of the monochromator, the following scheme was developed. For each angular range of interest (typically 1 keV for EXAFS scans) the position of the beam on the sample is checked. The pitch, roll and height of the second crystal stage are optimized for a few values within this energy domain, in such a way that the beam stays at a fixed

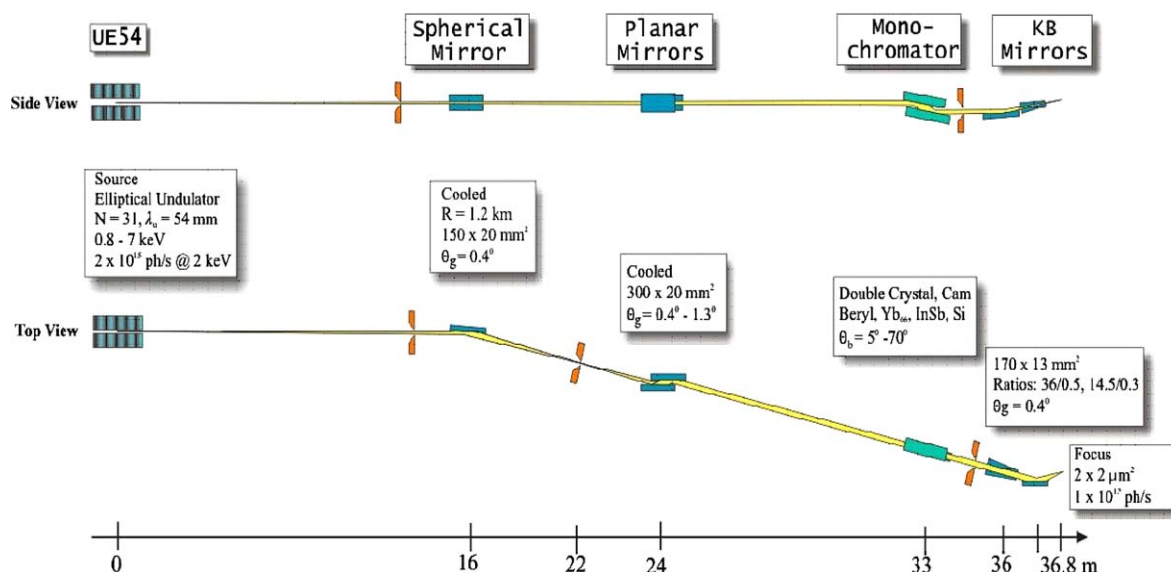


Fig. 1. Overall layout of the beamline.

position on the sample with the highest flux. The resulting values are then fitted by a five terms polynomial as a function of the energy. Finally, during an energy scan, the position of the second crystal is adjusted according to these functions at each point. So far the focused beam can be stabilized within 1  $\mu\text{m}$ .

The incident focused beam is monitored by measuring the total drain current of a polymer film coated with 50 nm of nickel, located at the exit of the KB system. Two Be windows separate the KB vessel and the end-station: one is fixed and its thickness is 7  $\mu\text{m}$ ; the other one, mounted on a valve, is 100  $\mu\text{m}$  thick. It can be opened when working in the low energy range. The experimental station vacuum can be as low as  $10^{-8}$  mbar, but in the high energy domain, by closing the thick Be window, experiments can be performed near atmospheric pressure. To obtain an optical image of the sample, two microscopes (wide and narrow fields) are looking through a viewport to a mirror located in front of the sample.

XAS spectra can be obtained by collecting the total electron yield as well as in the fluorescence mode. A mono-element energy dispersive silicon drift diode (SDD) is used, on which a special very thin window is mounted so that the fluorescence of elements down to the carbon can be detected. Its resolution is 120 eV at the Si K edge, 150 eV at the Ti K edge at count rate up to about 50 kHz. It can be translated on a linear slide to adjust the counting rate. Collecting data in the transmission mode is also possible by the use of a photo-diode positioned downstream behind the sample in the direct beam.

The samples are mounted on translation and rotation stages driven by stepping motors for translations down to 2  $\mu\text{m}$  and by piezo-electric stages for smaller displacements. Combined with XRF, this allows multielement cartography at the resolution of the photon spot size. In order to do that, several regions of interest (ROI) from the energy spectrum of the detector can be selected by the software

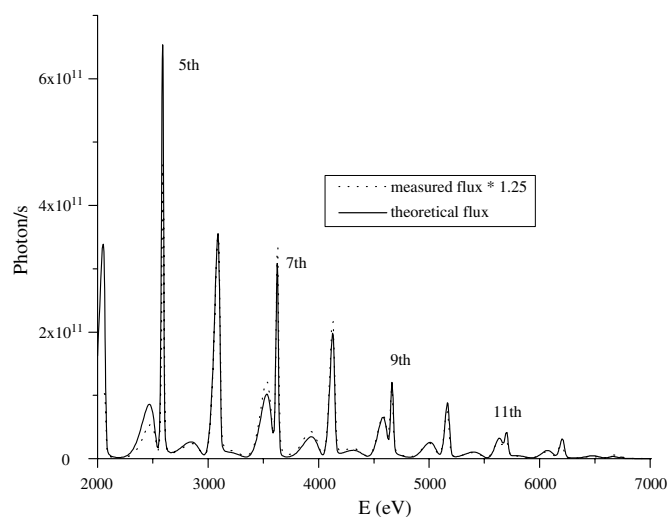


Fig. 2. Measured and calculated undulator spectrum at a gap of about 33 mm.

while the full energy spectrum is stored for each image point for further analysis.

### 3. Theoretical versus experimental

Fig. 2 compares a measured and a calculated spectrum of the flux provided by the undulator UE54 at a moderate gap setting of 33 mm. The experiment reaches 80% of the theoretically expected flux value. Thanks to its small phase error, the insertion device can be operated up to the 25th harmonic, enabling the acquisition of a full EXAFS scan above the iron K edge. Adjusting the undulator gap such that the energy of the X-ray monochromator always matches the maximum of the undulator peak (the so-called “undulator gap scan” technique), is routinely used. It provides a smooth profile of the incident X-rays. As an example, Fig. 3 shows Al K edge spectra measured using KTP as

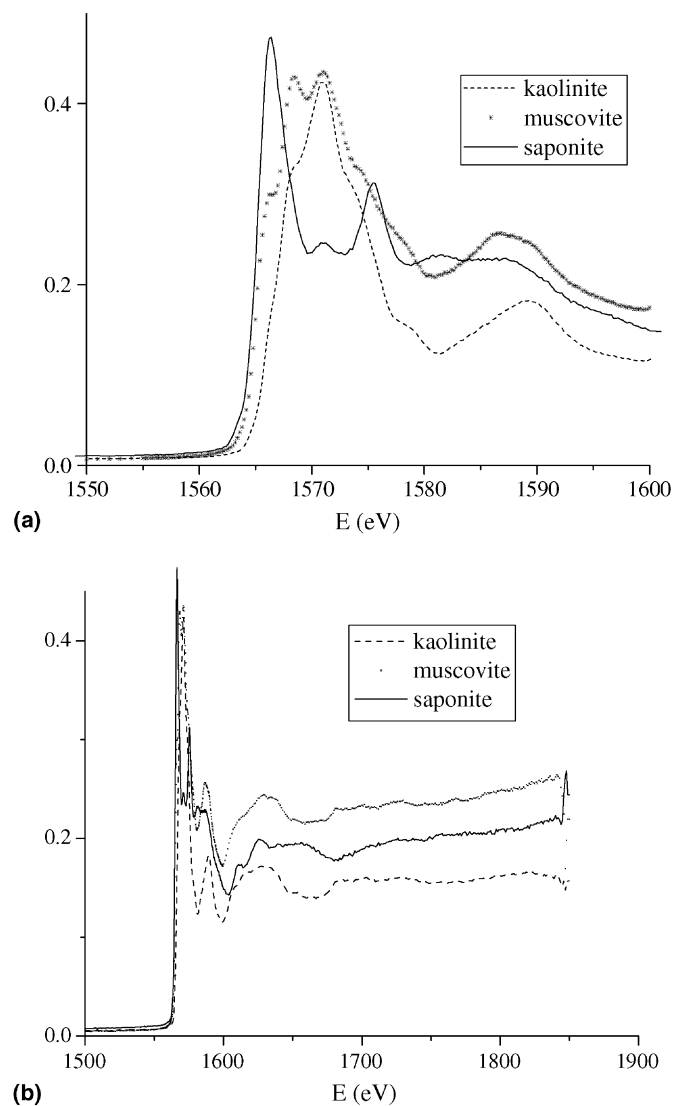


Fig. 3. Al K edge spectra for 4-fold coordinated Al (saponite), 6-fold coordinated Al (kaolinite), and 4- and 6-fold coordinated Al (muscovite). The spectra have been limited to 1840 eV because of the presence of silicon in the minerals.

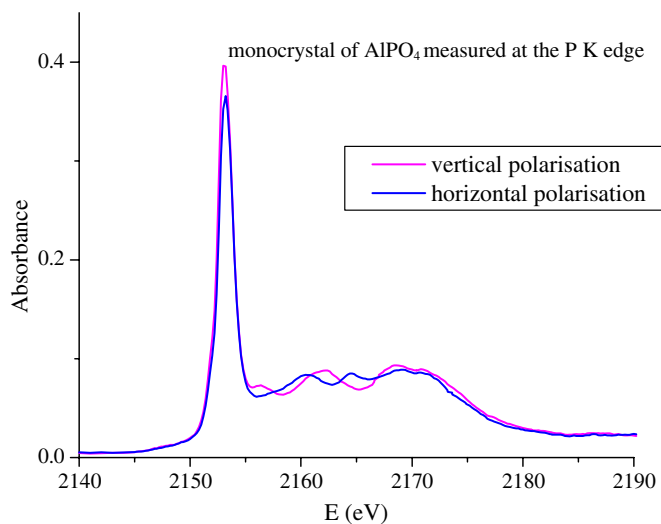


Fig. 4. Single crystal of  $\text{AlPO}_4$  measured at the P K edge with the polarization parallel to the  $c$ -axis (horizontal polarisation) or perpendicular to the  $c$ -axis (vertical polarisation). The signal was recorded by measuring the total drain current.

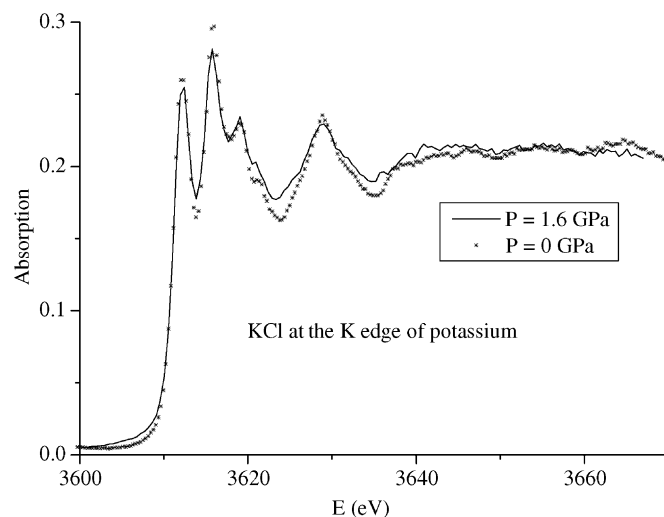


Fig. 5. X-ray absorption spectra of KCl at the potassium K edge measured in a diamond anvil cell at two different pressures. The spectrum at 1.6 GPa has been rescaled using the known equation of state of KCl.

monochromator crystals and measured by collecting the total drain current. As well the possibility offered by the

undulator of various polarization is shown in Fig. 4: the XANES spectra of a single crystal of  $\text{AlPO}_4$  at the P K

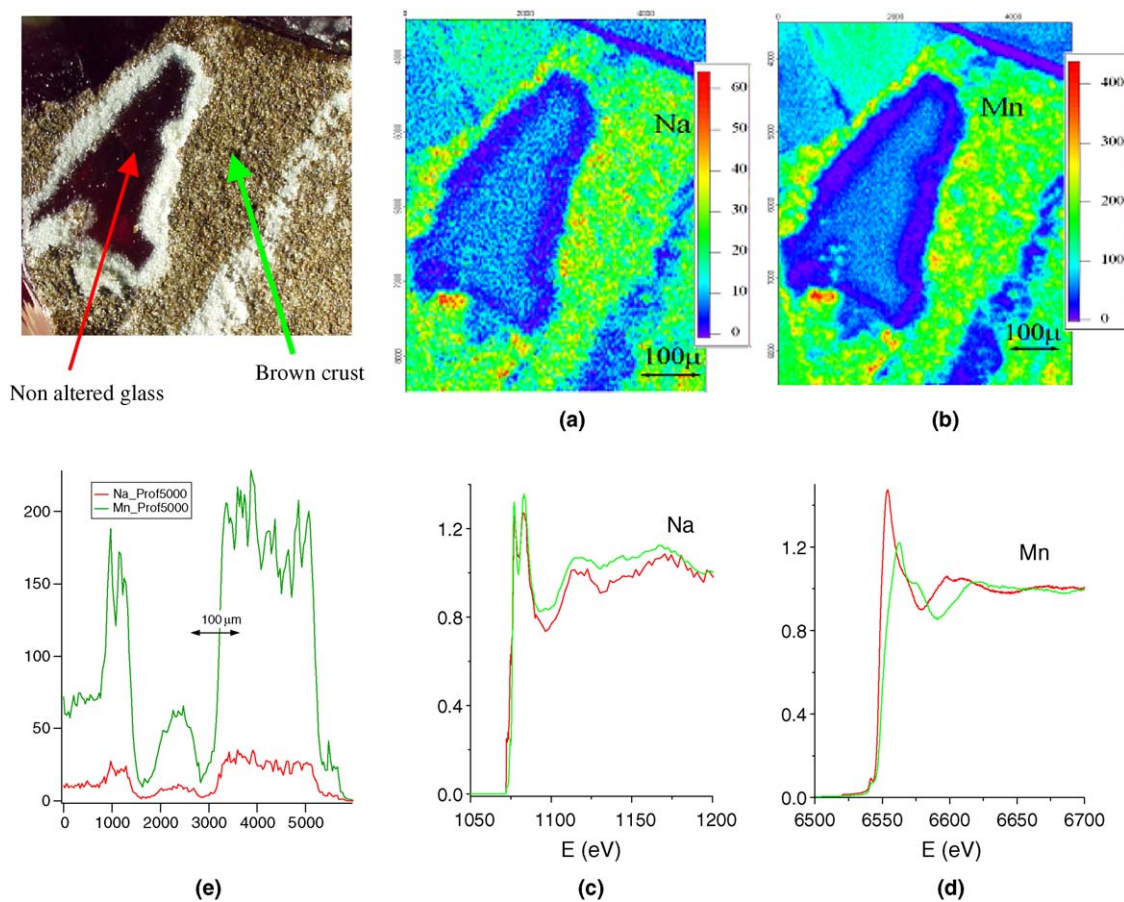


Fig. 6. Images of the Na (a) and Mn (b) repartition obtained on a Medieval glass of the Tours' cathedral (XIV century), and XANES spectra at the Na (c) and Mn (d) K-edges for two spots: (—) in the red non-altered glass (—) in the brown crust formed during alteration the line profiles (e) of the abundance of these two elements evidence their correlation, and the XANES spectra show the different speciation of Mn in these two parts of the glass. Is it a season impact or a bacterian effect? (For interpretation of the references in colour in this figure legend, the reader is referred to the web version of this article.)

edge with the polarization parallel or perpendicular to the  $c$ -axis present the expected linear dichroism already observed by rotating the sample versus the electric field. Therefore, polarization experiments can be performed on the same spot without moving the sample.

To simulate the theoretical performance of the KB focusing system, we performed ray-tracing simulations using SpotX, a software based on the Monte-Carlo method [5]. The calculated horizontal and vertical spot size were respectively  $3\ \mu\text{m}$  and  $0.4\ \mu\text{m}$  without slope errors, and  $4\ \mu\text{m}$  horizontally,  $2\ \mu\text{m}$  vertically, using the values of the slope errors measured on our LTP. The submicron size expected vertically is still difficult to obtain, and the minimum size achieved depends much on the quality of the X-ray beam at the entrance of the KB, related to the quality of the monochromator crystals. To measure the focal spot size, we conducted knife-edge scans through the focal spot, or performed mapping of Ti dots deposited on silicon wafers [6]. But this last method is only valid at high energies above the Ti K edge, for the Si(111) monochromator crystals. The smallest spot size obtained so far is  $2.5 (\pm 0.5) \times 2.5 (\pm 0.5)\ \mu\text{m}^2$  (H  $\times$  V, FWHM). We now aim at improving the vertical focusing. The photon flux in the focal spot measured with the photo-diode behind the KB

is  $>10^{10}$  photons per second per 100 mA in the energy range 0.8–8 keV.

#### 4. Initial results

The works described below show preliminary results: they have been carried out in collaboration with the first users of the beamline. They are mentioned here to illustrate the possibilities of the beamline over the full energy domain and they will be described in more details in dedicated papers.

##### 4.1. High pressure experiments at low energy [7]

X-ray absorption spectroscopy under high pressure was up to now limited to high energies edges (above 7 keV), because of the absorption of the diamond anvils used to achieve high pressure. The extension to low energy of these high pressure experiments has been one of the first experiments developed on LUCIA.

Two geometries for the high-pressure diamond anvil cell (DAC) are possible: with the incoming beam going through the partially perforated diamond, or through the Be gasket, while the fluorescence signal can be extracted through the

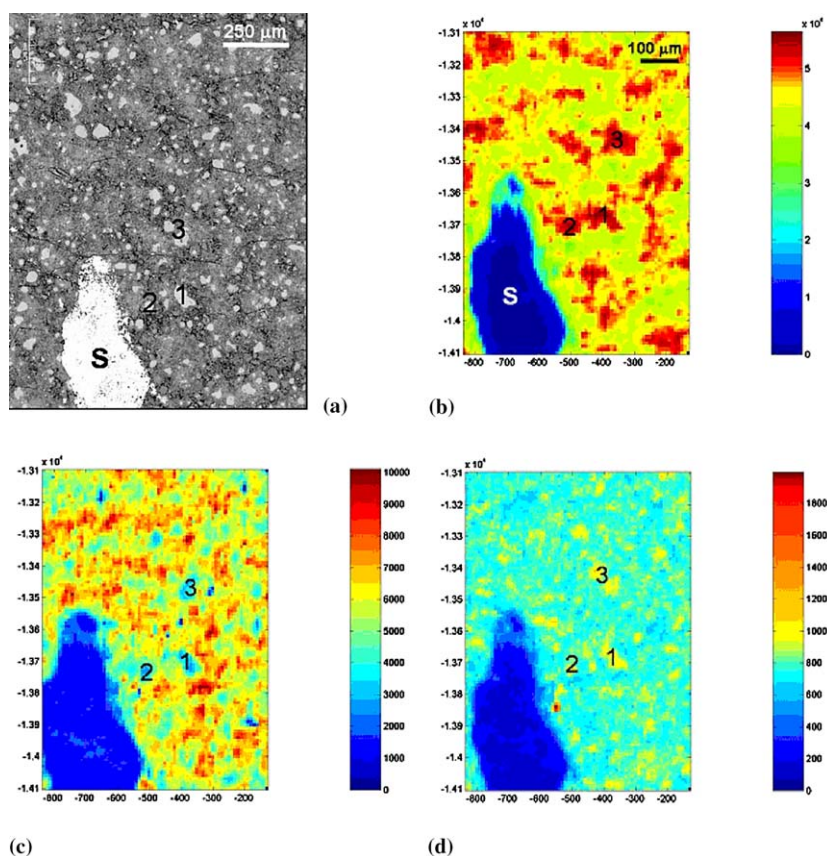


Fig. 7. (a) Back scatter electron (BSE) image of a 30 days hydrated cement.  $S$  = silver spot, used as a reference point; 1, 2 and 3 designate cement phases containing Ca and Si. XRF mapping of different elements from a 30 days hydrated cement collected at the SLS LUCIA beamline shown as follows: Ca (b), S (c) and Si (d). The  $X$ - and  $Y$ -axis show a micrometer scale, whereas the colorbar shows the intensities of each pixel with the corresponding counts. (For interpretation of the references in colour in this figure legend, the reader is referred to the web version of this article.)

gasket. Fig. 5 shows the K-edge spectrum of potassium in KCl taken in the DAC at two different pressures. The energy of the high pressure spectrum has been rescaled in order to take into account the bond length variation deduced from the equation of state and according to Natoli's rule,  $(E - E_0) * R^2 = cte$  [8]. With the interatomic distances assumed to follow the compressibility law of KCl, the agreement is quite satisfactory and validates the experiment.

#### 4.2. Study of medieval glasses exposed to weathering [9]

A series of XIV century medieval glasses from Tours and Strasbourg cathedrals stained-glass windows were studied by  $\mu$ -XRF and  $\mu$ -XAFS at the K-edges of Na, K, Ca, Mn, Fe and Cu, in order to understand first the origins of the color of the red glasses (Tours), as well as to study the formation of surface weathered phases for both the two sites. Glasses exposed to the outside suffered from corrosion (water, pollution, seasonal changes, etc.). They show surficial crusts enriched in manganese. The experiment is described in Fig. 6: the optical image select an interesting area, with unaltered glass and an altered part where complex compounds are formed. XRF mapping allows identifying the elements present in the different zones of the sample, and  $\mu$ -XRF gives the distribution of these elements. It was found that the distributions of Na and Mn are correlated, which infers the probable formation of a sodic birnesite that was not detected using conventional microscopic and diffraction studies. As confirmed by  $\mu$ -XANES experiments, the oxidation state of Mn is different in the different regions of the sample.

#### 4.3. Immobilization process of heavy metals in cement at the molecular level [10]

Cement-based materials play an important role in multi-barrier concepts developed worldwide for the safe disposal of industrial and radioactive wastes in underground repositories. Cement is used to condition the waste materials and to construct the engineered barrier systems (container, backfill and linear materials). Therefore, a mechanistic understanding of the processes governing the binding of heavy metals in cement systems is essential for long-term predictions of the environmental impact of cement-stabilized waste forms. Hardened cement paste (HCP) has been

investigated with the aim of improving the understanding of the immobilization process of heavy metals in cement at the molecular level. Fig. 7 is a part of such a study, where the first step is to understand the correlations between the distributions of the different elements present in this very heterogeneous material.

## 5. Conclusion

The LUCIA beamline is nowadays operating for almost one year since the first focused beam has been obtained on the experimental chamber end of May 2004. It is now open to users. The high quality of the undulator and the choice of a versatile monochromator and of a KB focusing system have allowed a full use of the stability of the SLS machine to obtain wide energy scans in the energy range from 0.8 up to 8 keV. Improvements have still to be done on the size of the photon spot, while the measured photon flux agrees well with the calculations. In the next future, an automated control of the bending of the KB mirrors should allow us a rapid and versatile tuning of the beam spot according to the willings of the users.

## References

- [1] T. Schmidt, F. Dubi, A. Imhof, B. Jakob, M. Janousch, A. Keller, A. Oggenfuss, R. Wetter, J. Bahrtdt, PSI Scientific report, Vol. VII, 2003, p. 25.
- [2] M. Lemonnier, O. Collet, C. Depautex, J.M. Esteva, D. Raoux, Nucl. Instr. and Meth. 152 (1) (1978) 109.
- [3] P. Kirkpatrick, A.V. Baez, J. Opt. Soc. Am. 38 (1948) 766.
- [4] L. Zhang, R. Hustache, O. Hignette, E. Ziegler, A. Freund, J. Synchrotron Rad. 5 (1998) 804.
- [5] T. Moreno, M. Idir, in: G. Jamelot et al. (Eds.), Proceedings of the 7th International Conference on X-Ray Lasers, J. Phys. IV, Vol. 11, 2001.
- [6] A.C. Thompson, J.H. Underwood, E.H. Anderson, S.A. McHugo, B. Lai, in: A.K. Freund et al. (Eds.), Proc. SPIE, Vol. 4145, 2001, p. 16.
- [7] Courtesy of J.P. Itie, IMPMC Paris, France (proposal number 20040292).
- [8] C.R. Natoli, in: A. Bianconi, L. Incoccia, S. Stipcich (Eds.), EXAFS and Near Edge Structure II, Springer Series in Chemical Physics, Vol. 27, Springer, Berlin, 1983, p. 43.
- [9] Courtesy of F. Farges (Université de Marne la Vallée), M.P. Etcheverry, I. Pallot Frossard (Laboratoire de Recherche des Monuments Historiques, France) (proposal number 20040284).
- [10] Courtesy of M. Vespa, A. Scheidegger, D. Grolimund, PSI, Switzerland (proposal number 20040317).